RSC Advances

PAPER

View Article Online
View Journal | View Issue

Cite this: *RSC Adv.*, 2016, **6**, 16177

N-Doped and Cu-doped TiO_2-B nanowires with enhanced photoelectrochemical activity†

Jingjie Su,‡[a] Zhaodong Li,‡[b] Yongquan Zhang,[c] Yingjin Wei*[c] and Xudong Wang*[ab]

Received 9th December 2015
Accepted 30th January 2016

DOI: 10.1039/c5ra26309c

www.rsc.org/advances

TiO_2-B is a metastable phase of titania with an interesting crystal structure and electrochemical properties. N-Doped and Cu-doped TiO_2-B nanowires (NWs) were synthesized by hydrothermal and microwave-assisted hydrothermal methods, respectively. All the NWs are single crystal with the same crystal orientation regardless of the synthesis method and doping situation. The doped NWs together with their corresponding pristine NWs were fabricated into a photoelectrochemical (PEC) anode for water oxidation and their photoactivity performances were studied and compared under different illumination wavelength ranges. The Cu-doped TiO_2-B NWs exhibited a significantly higher photocurrent density than all the other samples under direct Xe lamp illumination; while their performance rapidly dropped below the hydrothermal NWs when the UV illumination was cut off. On the contrary, N-doped TiO_2-B NWs exhibited significantly enhanced photoactivity particularly in the visible light range. X-ray photoelectron spectroscopy revealed that N-doping could narrow the electronic bandgap of TiO_2, while the Cu-doping had little impact on the bandgap but rather improved the electrical conductivity. This research provides a new insight into elemental and phase control of TiO_2-based solar energy harvesters.

1. Introduction

Titanium dioxide (TiO_2) is a promising photocatalyst material owing to its superior photostability, high intrinsic catalytic activity under UV illumination, and low cost.[1–3] Since the discovery of water photo-oxidation on TiO_2 photoanodes by Honda and Fujishima in 1972,[4] the application of TiO_2 in photoelectrochemical (PEC) water splitting has been attracting increasing attention. Most research nowadays is focused on the improvement of its catalytic performance. The wide bandgap (~3.0–3.2 eV) and poor electrical conductivity are generally known as the major limitations of TiO_2-based PEC anodes, which are hindering the increase of photoconversion efficiency. Doping TiO_2 crystals with foreign elements has been widely accepted and intensively studied as an effective approach to addressing both issues simultaneously. Many different types of doping elements (*e.g.* P, N, S, Nb, V, Fe, *etc.*)[5–14] or co-dopants (*e.g.* W–N, Fe–S, N–S, *etc.*)[15–17] have been investigated theoretically and experimentally to narrow the bandgap, improve the photoactivity in broad wavelength range, and enhance the overall solar energy conversion efficiency. Some of the doping strategies have demonstrated promising outcomes to largely improve the photocatalytic performance in visible light region.[5,8,18] Meanwhile, studies also showed that certain doping ions, such as N^{3-}, Nb^{5+}, and Sn^{4+} could appreciably enhance the electrical conductivity of TiO_2, which favorably impacted the electrochemical performance of TiO_2-based anodes of lithium ion batteries.[19–23]

Although researches on TiO_2 have been primarily focused on its rutile and anatase phases, the metastable bronze phase (known as TiO_2-B) is attracting more and more research interests due to its unique structural and electrochemical properties.[24,25] Compared to the anatase and rutile phases, TiO_2-B has a monoclinic crystal structure with a fairly opened three-dimensional lattice framework, rendering a large specific capacity and excellent rate capability for lithium ion battery applications.[26,27] However, due to its metastable nature with low thermodynamically stable temperature,[28] doping TiO_2-B to tune or improve its electronic property is more challenging than the other two phases. Recently, we successfully synthesized N-doped and Cu-doped TiO_2-B nanowires (NWs) by hydrothermal and microwave-based techniques.[26,29] Both N and Cu doping improved the charge transport property of TiO_2-B NWs as well as their cycle stability for lithium intercalation. Intrigued by the doping-induced superior electronic properties, it is intuitive to expect enhanced photocatalytic performance from the doped TiO_2-B NWs. In this paper, we report a systematic

[a]*Beijing Institute of Nanoenergy and Nanosystems, Chinese Academy of Sciences, National Center for Nanoscience and Technology (NCNST), Beijing 100083, China. E-mail: xudong.wang@wisc.edu*

[b]*Department of Materials Science and Engineering, University of Wisconsin-Madison, Madison, WI 53706, USA*

[c]*Key Laboratory of Physics and Technology for Advanced Batteries, Ministry of Education, College of Physics, Jilin University, Changchun 130012, P. R. China. E-mail: yjwei@jlu.edu.cn*

† Electronic supplementary information (ESI) available: XPS and XRD analysis results. See DOI: 10.1039/c5ra26309c

‡ These authors contributed equally.

study on the morphology- and doping-related PEC performance of both N-doped and Cu-doped TiO_2 NWs and compared to the undoped ones. Both doping materials demonstrated enhanced photoactivity, where Cu doping exhibited significantly enlarged overall photocurrent density (J_{ph}), while N-doping was found more favorable for visible light spectrum. This study offers new insights to TiO_2 materials design for high-performance photocatalysts development.

2. Experimental section

Synthesis of N-doped TiO_2-B NWs

Hydrothermal method was used to synthesize N-doped and corresponding pristine TiO_2-B NWs. Commercial TiN nanopowders (T110281, Aladdin) were used to prepare TiO_2 precursors. Prior to the synthesis, TiN nanopowders were heat treated at 400 °C in air for 10 hours (the heating time was variable to generate different N content in TiO_2 precursors). 0.4 g of the treated TiN nanopowders was dispersed in 40 mL of 10 mol L^{-1} NaOH solution. Then, the suspension was transferred into a 50 mL autoclave, which was sealed and heated at 170 °C for 60 hours. The autoclave was then naturally cooled down to room temperature and the precipitates were collected from suspension. The precipitates were dispersed in 0.1 mol L^{-1} of HCl solution and stirred at a constant rate for 4 hours yielding the desired titanate precipitates by proton exchange reactions. The titanate precipitates were washed by deionized (DI) water and centrifuged for three times, followed by freeze-drying at −30 °C under vacuum for 20 hours. The final products were annealed again at 450 °C for 4 hours under N_2 flow to improve the crystallinity. The pristine TiO_2 NWs were synthesized through the same procedure but only a higher pre-heat treatment temperature (500 °C) was applied. The appropriate annealing temperature is the key for the formation of high quality and well-crystallized TiO_2-B phase NWs.

Synthesis of Cu-doped TiO_2-B NWs

The Cu-doped and corresponding pristine TiO_2-B NWs were synthesized by the microwave-assisted hydrothermal method. 0.5 g of TiO_2 (P25, Degussa) and $Cu(NO_3)_2 \cdot 3H_2O$ (3 mol% respect to TiO_2) were dispersed in 60 mL of 10 mol L^{-1} KOH solution. Similar to the preparation of N-doped TiO_2-B NWs, the suspension was transferred into a 100 mL autoclave, which was sealed and heated at 200 °C for 90 min. The entire heating process was conducted under a 500 W microwave irradiation. The autoclave was then naturally cooled down to room temperature, and the precipitates ($K_2Ti_{8-x}Cu_xO_{17}$) were collected from the solution. The obtained precipitates were dispersed in 0.1 mol L^{-1} HNO_3 solution with stirring for 4 hours, where the K^+ ions were extracted *via* proton exchange reactions. The new precipitates ($H_2Ti_{8-x}Cu_xO_{17}$) were dispersed in 60 mL of 0.1 mol L^{-1} HNO_3 solution and transferred to the autoclave for microwave heat treatment again (180 °C for 90 min). After the autoclave was naturally cooled down to room temperature, the precipitates were collected by centrifuging and washing with DI water. Finally, the products were freeze-dried at −30 °C under vacuum for 20 hours, and then heat treated at 400 °C for 2 hours under N_2 flow. The pristine TiO_2-B NWs were synthesized *via* the same procedure without using the $Cu(NO_3)_2 \cdot 3H_2O$ precursor.

Characterization of TiO_2-B NWs

The morphology of TiO_2-B NWs was characterized by LEO 1530 Gemini scanning electron microscopy (SEM, Zeiss, Germany). The chemical compositions were characterized by X-ray photoelectron spectroscopy (XPS, Thermo Fisher Scientific Inc., Waltham, MA). The survey binding energy range was from 0 to 1350 eV, where the density of states (DOS) of the valence band maximum (VBM) profile was also derived. In addition, Tecnai TF-30 transmission electron microscopy (TEM, FEI, OR) was conducted to obtain the crystallography and lattice information. X-ray diffraction (XRD) was performed on the powder samples using Bruker D8 Discovery facility (Bruker, MA).

PEC photoanode preparation and characterization

The TiO_2-B NWs were dispersed into the *tert*-butanol (Sigma-Aldrich, St. Louis, MO) with the weight ratio of 1 to 6, and stirred for 3 hours. The obtained paste was then applied onto fluorine doped tin oxide (FTO) glass substrates to a thickness of ~20 μm. The paste film was hardened by 2 hour heat treatment at 200 °C in the air. The hardened TiO_2-B NW films were sealed by epoxy, leaving an exposed active area of ~0.22 mm^2 as the active photoanode surface. PEC measurements were performed by a three-electrode electrochemical cell configuration, using a 30 mL aqueous solution of 1 mol L^{-1} KOH (pH = 14). A Pt wire served as the counter electrode, and a saturated calomel electrode (SCE) served as the reference electrode. All electrodes were connected to a potentiostat system (Metrohm Inc., Riverview, FL) for the PEC measurements. Light illumination was provided by a 150 W Xe arc lamp (Newport Corporation, Irvine, CA), and the intensity at the PEC photoanode position was adjusted to be 100 mW cm^{-2}. An AM 1.5G filter and a UV cutoff filter were also utilized with the lamp to control the illumination wavelength.

3. Results and discussion

Fig. 1a and b show the SEM images of the pristine and N-doped TiO_2-B NWs prepared by the hydrothermal method, respectively. The pristine TiO_2-B NWs exhibited a size of 60–110 nm in diameter and up to ten microns in length. In contrary, the diameter of the N-doped NWs was decreased to 30–95 nm and a larger number of shorter NWs were observed. The reduced growth rates were typically observed from extrinsically doped nanostructures due to the poisoning effect from foreign elements. The TiO_2-B NWs made from microwave-assisted approach demonstrated a much smaller diameter, typically less than 10 nm with an fairly large aspect ratio (up to ~1000), as shown in Fig. 1c. Cu doping imposed no obvious change to the geometry of the NWs, as shown in Fig. 1d, possibly due to the already very small thickness. The extremely small diameter of the TiO_2-B NWs from the microwave approach was likely a result of the heating pattern from microwave irradiation.

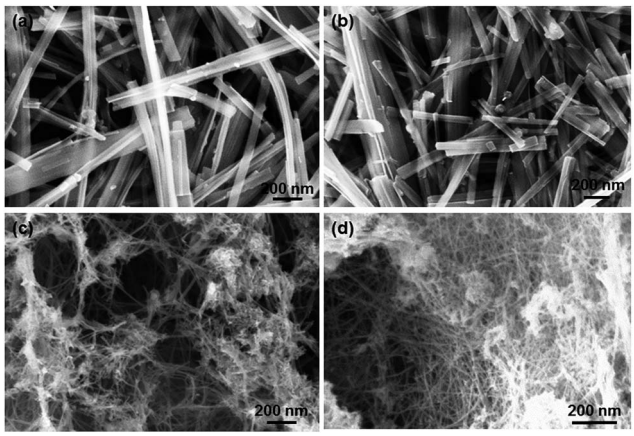

Fig. 1 Morphologies of TiO_2 NWs synthesized by different methods. (a) Undoped and (b) N-doped TiO_2-B NWs from hydrothermal method. (c) Undoped and (d) Cu-doped TiO_2-B NWs from microwave-assisted hydrothermal method.

Concentrated heat from microwave could yield very high precursor concentration locally, which was favorable for rapid nucleation with uniform and small nuclei.

TEM was further implemented to study the NWs morphologies and crystal structures. Fig. 2 compared the crystallography of pristine and N-doped TiO_2-B NWs prepared by hydrothermal method. Fig. 2a shows a single pristine TiO_2-B NW with a diameter of ~200 nm. Small wire-like branches could also be observed attaching along its side surface. Nevertheless, the entire NW appeared to be a single crystal, as supported by the selected area electron diffraction (SAED) pattern shown in Fig. 2b. It revealed that the NW was grown along the [010] direction and the side facets are (100) planes. High resolution TEM (HRTEM) taken from the NW showed a clear single crystal lattice, where the lattice constants of the (110) and (100) facets were measured to be 0.34 and 0.80 nm, respectively (Fig. 2c). Corresponding fast Fourier transform (FFT) of the crystal lattice demonstrated an identical pattern as the SAED (Fig. 2d). The N-doped NWs were obvious smaller in size, as shown in Fig. 2e; while they were still single crystal with the same growth orientation as indicated by the SAED pattern (Fig. 2f). No detectable lattice constant change could be identified from the HRTEM image (Fig. 2g) and corresponding FFT pattern (Fig. 2h). However, distortions of crystal lattices were observed from the HRTEM image as a possible result of N doping (Fig. 2g).

Pristine TiO_2-B NWs synthesized *via* the microwave-assisted growth were shown in Fig. 3a. The NWs were mostly ~5 nm in diameter but were broken into small pieces due to sample preparation. HRTEM and corresponding FFT pattern clearly revealed the single-crystalline feature of the NWs, showing they were growing along the [010] direction (Fig. 3b). Since the lattice constant of the (100) plane is 0.8 nm, there were only 5–6 atomic layers along the thickness direction, yielding the total thickness of 4–5 nm. The Cu-doped TiO_2 NWs exhibited very similar thickness distribution as the pristine ones (Fig. 3c). They exhibited single-crystalline lattice from HRTEM image (Fig. 3d) with the same growth direction and side surfaces. However, several concentric broad diffraction rings were also shown in

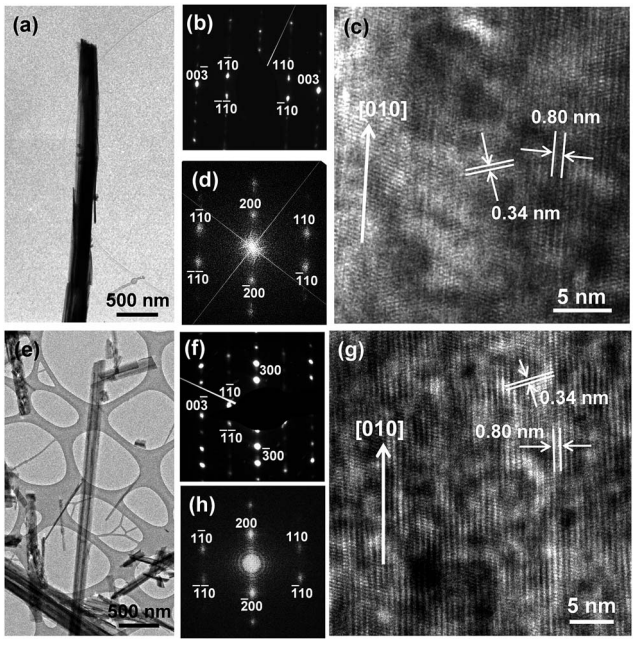

Fig. 2 Crystal structures of undoped and N-doped TiO_2 NWs synthesized by hydrothermal method. (a) TEM image of a single undoped TiO_2-B NW. (b) SAED pattern taken from the NW shown in (a). (c) HRTEM image taken from the body region of the TiO_2-B NW revealing its good crystallinity. (d) FFT pattern of the lattice image shown in (c). (e and f) TEM image (e) and corresponding SAED pattern (f) of N-doped TiO_2-B NWs. (g) HRTEM image showing a single-crystalline structure with distorted lattices possibly due to N doping. (h) FFT pattern of the lattice image shown in (g).

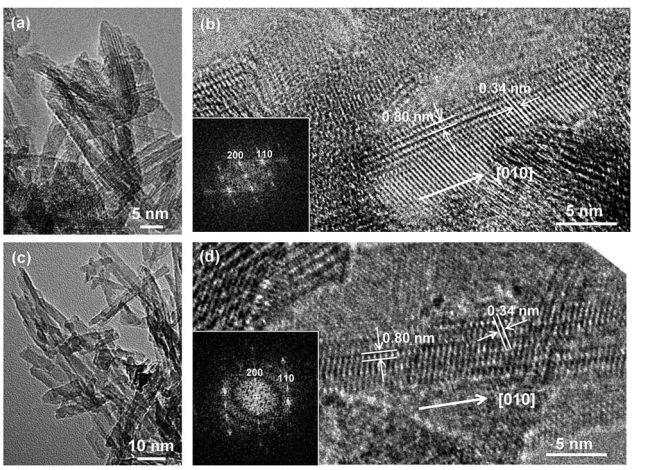

Fig. 3 TEM images of undoped and Cu-doped TiO_2 NWs synthesized by microwave-assisted method. (a) TEM image present the prepared TiO_2 NWs as tiny as ~4 nm in diameter. (b) High resolution TEM image shows a good crystallization of the NWs. Inset is the FFT pattern taken from the lattice image. It confirms the anatase phase. (c) The TEM image and (d) high resolution TEM image also indicate the highly crystallized small TiO_2 NWs after Cu doping. Inset FFT pattern confirms the anatase phase of Cu-doped TiO_2 NWs.

the FFT pattern (inset of Fig. 2d), suggesting that the Cu-doped sample might have low crystallinity in certain area. In general, the TEM analysis verified that all the TiO_2 NWs are the bronze phase with the same crystal orientation, but the crystallinity of the TiO_2-B NWs prepared by the hydrothermal method might be higher.

X-ray photoelectron spectroscopy (XPS) was implemented to study the elemental characteristics of the doped and pristine TiO_2-B NWs samples synthesized by both methods (the full spectra are shown in Fig. S1†). To analyze the chemical structures of the N-doped TiO_2-B NWs, three regions of the XPS spectrum were investigated: O 1s scan near 530 eV, Ti 2p scan near 460 eV, and N 1s scan near 400 eV. The deconvoluted spectra for the O 1s, Ti 2p and N 1s peaks are shown in Fig. 4a. For comparison, these spectra from pristine hydrothermal TiO_2-B NWs were also analyzed (Fig. S2a†). The N 1s peak was clearly shown by the N-doped NWs but absent in undoped sample. In the O 1s profile of N-doped NWs, the surface OH group related peak at 532.4 eV was replaced by the peak related with O–Ti–N bound at 531.3 eV. The appearance of O–Ti–N bound evidenced the substitution of O atoms by N atoms. The approximated proportion of the substituted-dopant in the N-doped TiO_2-B can be quantified through linear correlation between O–Ti–N peak area and integral of the O 1s spectrum, which is about 8.63%.[30] In addition, research has shown that when O was replaced by N, the valence state of Ti cation would be reduced from Ti^{4+} to Ti^{3+}, making the binding energy of the Ti $2p_{3/2}$ peak shift to lower energies.[31,32] As shown in the deconvoluted spectra of the Ti 2p peaks in Fig. 4a, Ti^{3+} signals appeared at 458.3 eV in Ti $2p_{3/2}$ (green) and 463.5 eV in Ti $2p_{1/2}$ (purple), which were located at the lower binding energy side of each Ti–O peak. In contrast, only two typical Ti–O peaks were observed from the undoped sample (Fig. S2a†). Above comparisons of XPS spectra confirmed a successful incorporation of N in the TiO_2-B NWs lattice.

Likewise, the chemical structures of Cu-doped and pristine TiO_2-B NWs by microwave-assisted approach were also studied based on their XPS spectra, as shown in Fig. 4b and S2b†, respectively. First of all, the characteristic Cu $2p_{3/2}$ and $2p_{1/2}$ peaks were observed at 932.6 eV and 952.1 eV, respectively, which are consistent with those of the Cu^{2+} cations.[33] These peaks were absent from the pristine NWs sample, confirming the successful doping of Cu into TiO_2-B NWs. Similar deconvoluted spectra of O 1s peaks were observed. Surface OH group was found from both types of NWs. The amount of surface OH group could be derived from the area ratio of the OH group peak to the entire O 1s peak. The area ratio of Cu-doped NWs was ~6.2% compared to ~5.2% of the pristine NWs, indicating that Cu-doping could induce more surface absorbed OH groups. In addition, different from the N-doped TiO_2-B NWs, the Ti $2p_{3/2}$ (458.6 eV) and Ti $2p_{1/2}$ (464.3 eV) exhibited a fairly symmetric shape in the Cu-doped sample and Ti^{3+} peaks could not be convincingly distinguished from deconvolution. This suggests that Cu cation might be interstitially doped into the TiO_2-B lattice.[34]

Both N-doped and Cu-doped TiO_2-B NWs were made into PEC photoanode with 2 hour heat treatment at 200 °C in the air (see experiment session for details). The XRD results in Fig. S3† illustrate that the phases of obtained TiO_2-B NWs were very stable during this thermal process. The PEC performance of both N-doped and Cu-doped TiO_2-B NWs were then characterized for water oxidation in 1 mol L^{-1} KOH electrolyte and compared with their corresponding pristine TiO_2 NWs samples and commercial P25 TiO_2 nanopowders. Fig. 5 shows the plots of J_{ph} *versus* bias potential (V) of all samples under illumination of a 100 W cm^{-2} Xe lamp without and with AM 1.5G or UV cutoff filter. The dark current densities of each PEC test remained at a very low level within the entire bias potential range (*vs.* SCE). As shown in Fig. 5a, when the direct Xe lamp was used as the illumination source, which contains a large portion of UV spectrum, the Cu-doped TiO_2-B NWs exhibited a significantly higher J_{ph} (0.8 mA cm^{-2} at 0.5 V *vs.* SCE, the rest J_{ph} values were all collected at this bias) than other three TiO_2-B NWs samples (all ranged between 0.11–0.17 mA cm^{-2}). Among the rest, N-doped TiO_2-B NWs had a slightly higher J_{ph} than the two undoped ones. Nevertheless, all the TiO_2-B NWs exhibited obviously higher J_{ph} than the rutile P25 TiO_2 nanopowders (only 0.03 mA cm^{-2}).

When these samples were illuminated under AM 1.5G solar spectrum, their J_{ph} were all dropped to lower values due to the largely reduced UV lights (Fig. 5b). Among them, the Cu-doped NWs still exhibited the highest J_{ph} (0.17 mA cm^{-2}) but the ratio of enhancement was much less compared to the Xe-lamp case. However, enhancement from the N-doped NWs became more obvious, which was 0.08 mA cm^{-2} and twice as much as that from the undoped hydrothermal-synthesized NWs. The undoped microwave-synthesized TiO_2 NWs still exhibited the lowest J_{ph} (0.02 mA cm^{-2}), which was ~8.5 and ~4 times smaller than the Cu-doped and N-doped NWs, respectively. This comparison revealed that the enhancement ratio between Cu-doped and pristine TiO_2-B NWs by the microwave method was nearly unchanged before and after applying the AM 1.5G filter. Nonetheless, the N-doped sample exhibited a significantly larger J_{ph} improvement ratio when the illumination was switched to AM 1.5G. This phenomenon suggests that N-doped

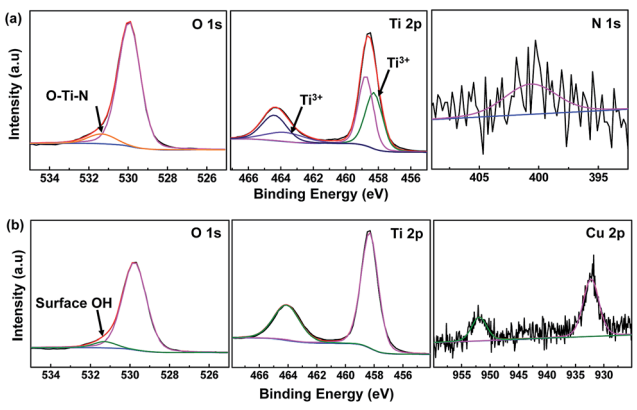

Fig. 4 Deconvoluted XPS spectra for (a) O 1s peak, Ti 2p peak, and Cu 2p peak of N-doped TiO_2 NWs by hydrothermal method and (b) O 1s peak, Ti 2p peak, and Cu 2p peak of Cu-doped TiO_2 NWs by microwave-assisted method.

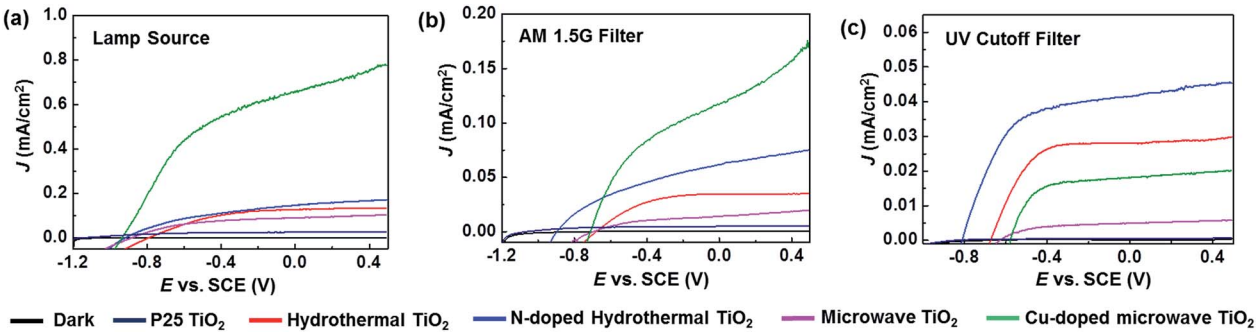

Fig. 5 (a–c) J–V curves of undoped and N-doped TiO_2 NWs, as well as the undoped and Cu-doped TiO_2 NWs under illuminations of 100 mW cm^{-2} Xe lamp source, lamp with AM 1.5G filter, and lamp with UV cut off filter, respectively. The P25 TiO_2 nanopowder was also prepared as the reference sample.

TiO_2-B NWs were much more sensitive to light in the visible wavelength regime. This argument was further supported by the J_{ph} measurements under visible light illumination, where all photons with wavelength smaller than 400 nm were blocked. As shown in Fig. 5c, under this condition, the N-doped TiO_2-B NWs exhibited the highest J_{ph}, followed by their corresponding undoped hydrothermal NWs. J_{ph} of Cu-doped TiO_2-B NWs was dropped to only 40% of the J_{ph} of the N-doped NWs and 67% of the undoped hydrothermal NWs, while it was still 3.3 times higher than the undoped microwave TiO_2-B NWs. This fact also revealed that Cu-doping has limited influence on the visible-light photoactivity. Its enhancement effect may be largely attributed by the improved conductivity.[35]

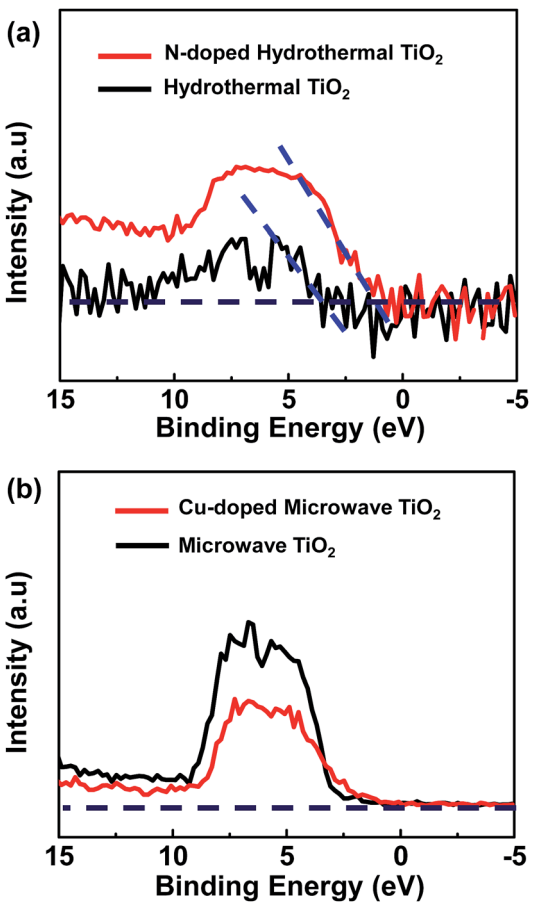

Fig. 6 XPS spectra demonstrates that density of states (DOS) shift in the valence band happened to both N-doped TiO_2 NWs prepared by hydrothermal method (a) and Cu-doped TiO_2 NWs prepared by microwave-assisted method (b) compared to the undoped samples prepared by the same method. The maximum shift is ~2.45 eV in N-doped TiO_2 NWs and ~1.56 eV in Cu-doped TiO_2 NWs.

Shift of the density of states (DOS) of the valence band was extracted from the XPS spectra and further confirmed the influences of doping elements to the electronic and optical properties of TiO_2-B NWs. As shown in Fig. 6a, the undoped hydrothermal TiO_2-B NWs had a valance band maximum (VBM) at ~3.7 eV; while the N-doped NWs exhibited a VBM at ~1.2 eV, representing a shift of 2.5 eV due to N-doping. Such a significant bandgap narrowing was consistent to other N-doped TiO_2 nanostructures with either anatase or rutile phases. It could introduce appreciably enhanced photoactivity in visible light regime. On the contrary, Cu-doped TiO_2-B NWs didn't show obvious VBM shift (Fig. 6b), which is in accordance with the weak enhancement of the visible light photoactivity by Cu-doping.

4. Conclusions

In summary, the N-doped and Cu-doped TiO_2-B NWs were synthesized by the hydrothermal method and microwave-assisted hydrothermal method, respectively. Due to the different growth conditions, particularly different heating pattern, the as-synthesized NWs exhibited different morphology, where the microwave-assisted hydrothermal process yielded fairly small NWs with extremely large aspect ratio. Regardless of the synthesis methods and doping situation, all the NWs exhibited a single crystalline bronze phase with the same growth orientation. The successful doping of N and Cu elements was supported by XPS analysis. PEC performance was measured for the doped and corresponding pristine TiO_2-B NWs under different illumination spectra. Cu-doped NWs exhibited extraordinarily higher J_{ph} compared to all the other samples when the UV light portion was large in the spectrum. The performance of N-doped NWs rose to the top

under visible light illumination. Our experiment revealed that N doping consistently narrowed the bandgap of TiO_2-B NWs and significantly improved their visible light photoactivity. Cu-doping had very limited effect to the bandgap and the improvement could largely be attributed to its conductivity improvement. This research provides a new insight to the doping effect of the TiO_2-B phase. It demonstrated a promising strategy of material design and phase control of TiO_2-based photocatalysts that are active within a broad wavelength range.

Acknowledgements

The authors thank the support of the "Thousands talents" program for pioneer researcher and his innovation team, China.

References

1 X. Chen and S. S. Mao, *Chem. Rev.*, 2007, **107**, 2891–2959.
2 R. Asahi, T. Morikawa, T. Ohwaki, K. Aoki and Y. Taga, *Science*, 2001, **293**, 269–271.
3 R. Leary and A. Westwood, *Carbon*, 2011, **49**, 741–772.
4 A. Fujishima and K. Honda, *Nature*, 1972, **238**, 37–38.
5 R. Asapu, V. M. Palla, B. Wang, Z. H. Guo, R. Sadu and D. H. Chen, *J. Photochem. Photobiol., A*, 2011, **225**, 81–87.
6 M. C. Wu, J. Hiltunen, A. Sapi, A. Avila, W. Larsson, H. C. Liao, M. Huuhtanen, G. Toth, A. Shchukarev, N. Laufer, A. Kukovecz, Z. Konya, J. P. Mikkola, R. Keiski, W. F. Su, Y. F. Chen, H. Jantunen, P. M. Ajayan, R. Vajtai and K. Kordas, *ACS Nano*, 2011, **5**, 5025–5030.
7 T. Ohno, M. Akiyoshi, T. Umebayashi, K. Asai, T. Mitsui and M. Matsumura, *Appl. Catal., A*, 2004, **265**, 115–121.
8 C. Das, P. Roy, M. Yang, H. Jha and P. Schmuki, *Nanoscale*, 2011, **3**, 3094–3096.
9 B. S. Liu, X. L. Wang, G. F. Cai, L. P. Wen, Y. B. Song and X. J. Zhao, *J. Hazard. Mater.*, 2009, **169**, 1112–1118.
10 S. Sood, A. Umar, S. K. Mehta and S. K. Kansal, *J. Colloid Interface Sci.*, 2015, **450**, 213–223.
11 J. C. Xu, M. Lu, X. Y. Guo and H. L. Li, *J. Mol. Catal. A: Chem.*, 2005, **226**, 123–127.
12 G. M. Wang, X. H. Xiao, W. Q. Li, Z. Y. Lin, Z. P. Zhao, C. Chen, C. Wang, Y. J. Li, X. Q. Huang, L. Miao, C. Z. Jiang, Y. Huang and X. F. Duan, *Nano Lett.*, 2015, **15**, 4692–4698.
13 J. X. Xu, C. Chen, X. H. Xiao, L. Liao, L. Miao, W. Wu, F. Mei, A. L. Stepanov, G. X. Cai, Y. Liu, Z. G. Dai, F. Ren, C. Z. Jiang and J. R. Liu, *J. Appl. Phys.*, 2014, **115**, 143106.
14 S. Hoang, S. P. Berglund, N. T. Hahn, A. J. Bard and C. B. Mullins, *J. Am. Chem. Soc.*, 2012, **134**, 3569–3662.
15 X. Li, Y. Y. Liu, P. F. Yang and Y. C. Shi, *Particuology*, 2013, **11**, 732–736.
16 G. D. Yang, Z. Jiang, H. H. Shi, M. O. Jones, T. C. Xiao, P. P. Edwards and Z. F. Yan, *Appl. Catal., B*, 2010, **96**, 458–465.
17 M. Sathish, R. P. Viswanath and C. S. Gopinath, *J. Nanosci. Nanotechnol.*, 2009, **9**, 423–432.
18 Y. F. Shen, T. Y. Xiong, J. K. Shang and K. Yang, *Res. Chem. Intermed.*, 2008, **34**, 353–363.
19 N. A. Kyeremateng, F. Vacandio, M. T. Sougrati, H. Martinez, J. C. Jumas, P. Knauth and T. Djenizian, *J. Power Sources*, 2013, **224**, 269–277.
20 J. G. Kim, D. Q. Shi, K. J. Kong, Y. U. Heo, J. H. Kim, M. R. Jo, Y. C. Lee, Y. M. Kang and S. X. Dou, *ACS Appl. Mater. Interfaces*, 2013, **5**, 691–696.
21 Y. M. Li, Z. G. Wang and X. J. Lv, *J. Mater. Chem. A*, 2014, **2**, 15473–15479.
22 Y. Q. Zhang, F. Du, X. Yan, Y. M. Jin, K. Zhu, X. Wang, H. M. Li, G. Chen, C. Z. Wang and Y. J. Wei, *ACS Appl. Mater. Interfaces*, 2014, **6**, 4458–4465.
23 Y. D. Wang, T. Chen and Q. Y. Mu, *J. Mater. Chem.*, 2011, **21**, 6006–6013.
24 J. Dai, J. Yang, X. H. Wang, L. Zhang and Y. J. Li, *Appl. Surf. Sci.*, 2015, **349**, 343–352.
25 M. Fehse and E. Ventosa, *ChemPlusChem*, 2015, **80**, 785–795.
26 Y. Q. Zhang, Q. Fu, Q. L. Xu, X. Yan, R. Y. Zhang, Z. D. Guo, F. Du, Y. J. Wei, D. Zhang and G. Chen, *Nanoscale*, 2015, **7**, 12215–12224.
27 V. Mansfeldova, B. Laskova, H. Krysova, M. Zukalova and L. Kavan, *Catal. Today*, 2014, **230**, 85–90.
28 M. Kobayashi, V. V. Petrykin and M. Kakihana, *Chem. Mater.*, 2007, **19**, 5373–5376.
29 Y. Q. Zhang, Y. Meng, K. Zhu, H. L. Qiu, Y. M. Ju, Y. Gao, F. Du, B. Zou, G. Chen and Y. J. Wei, *ACS Appl. Mater. Interfaces*, 2015, in revision.
30 F. Larachi, J. Pierre, A. Adnot and A. Bernis, *Appl. Surf. Sci.*, 2002, **195**, 236–250.
31 X. B. Chen and C. Burda, *J. Phys. Chem. B*, 2004, **108**, 15446–15449.
32 S. Hashimoto and A. Tanaka, *Surf. Interface Anal.*, 2002, **34**, 262–265.
33 K. E. Elers, J. Winkler, K. Weeks and S. Marcus, *J. Electrochem. Soc.*, 2005, **152**, G589–G593.
34 F. Peng, L. F. Cai, H. Yu, H. J. Wang and J. Yang, *J. Solid State Chem.*, 2008, **181**, 130–136.
35 H. M. Yadav, S. V. Otari, V. B. Koli, S. S. Mali, C. K. Hong, S. H. Pawar and S. D. Delekar, *J. Photochem. Photobiol., A*, 2014, **280**, 32–38.

